Title

Brain hypothyroidism silences the immune response of microglia in Alzheimers disease animal model.

Journal

Science Advances, 10(11)

Authors

Kim, Dong
Choi, Hyunjung
Lee, Woochan
et al.

Publication Date

2024-03-15

DOI

10.1126/sciadv.adi1863

Peer reviewed

NEUROSCIENCE

Brain hypothyroidism silences the immune response of microglia in Alzheimer's disease animal model

Dong Kyu Kim[1,2]†, Hyunjung Choi[2,3]†, Woochan Lee[1], Hayoung Choi[1,2], Seok Beom Hong[1,2], June-Hyun Jeong[1,2], Jihui Han[1,2], Jong Won Han[1,2], Hoon Ryu[4], Jong-Il Kim[1], Inhee Mook-Jung[1,2,3]*

Thyroid hormone (TH) imbalance is linked to the pathophysiology of reversible dementia and Alzheimer's disease (AD). It is unclear whether tissue hypothyroidism occurs in the AD brain and how it affects on AD pathology. We find that decreased iodothyronine deiodinase 2 is correlated with hippocampal hypothyroidism in early AD model mice before TH alterations in the blood. TH deficiency leads to spontaneous activation of microglia in wild-type mice under nonstimulated conditions, resulting in lowered innate immune responses of microglia in response to inflammatory stimuli or amyloid-β. In AD model mice, TH deficiency aggravates AD pathology by reducing the disease-associated microglia population and microglial phagocytosis. We find that TH deficiency reduces microglial ecto-5′-nucleotidase (CD73) and inhibition of CD73 leads to impaired innate immune responses in microglia. Our findings reveal that TH shapes microglial responses to inflammatory stimuli including amyloid-β, and brain hypothyroidism in early AD model mice aggravates AD pathology by microglial dysfunction.

INTRODUCTION

Alzheimer's disease (AD) is the most common cause of dementia, accounting for up to 80% of all dementia cases (*1*). Although some early-onset cases are associated with inherited genetic abnormalities, these constitute 1% or less of all AD cases. Most late-onset cases are characterized by a gradual decline in cognitive function over years (*2*–*4*). In most studies, two distinct lesions in the brain, amyloid plaques and neurofibrillary tangles, are required for a neuropathological diagnosis of AD (*5*). It has also been reported that AD pathogenesis can result from complicated pathological alterations caused by mitochondrial malfunction, abnormal Ca^{2+} dysregulation, oxidative stress, neuroinflammation, and metabolic abnormalities (*6*–*12*).

Thyroid hormones (THs) are fundamental determinants of metabolic activity and the development of the brain (*13*). The concentrations of THs in the brain are tightly regulated by homeostatic mechanisms, indicating that THs are essential for the preservation of brain function throughout life. The hypothalamus-pituitary-thyroid axis is in charge of TH production and is regulated by two primary THs: thyroxine (T_4), a prohormone produced by the thyroid gland, and triiodothyronine (T_3), the bioactive form produced by conversion of T_4 via deiodinase in the brain (*14*). Several studies have shown that the failure of TH homeostatic regulation disrupts gene expression modulated by TH-mediated activation of TH receptors, affecting neural cell migration and differentiation, synaptogenesis, and myelination (*15*) and contributing to the etiology of various neurological pathologies such as multiple sclerosis, traumatic brain injury, and Parkinson's disease (*16*–*19*).

A variety of epidemiological studies on TH levels in patients with AD have been conducted to investigate the effects of these hormones on the incidence and progression of AD. Subclinical thyroid dysfunction [i.e., elevated or reduced thyroid-stimulating hormone (TSH) levels with normal T_3 and T_4] has been linked to cognitive impairment and is a risk factor for dementia (*20*, *21*). Other studies have reported that serum TSH levels in patients with euthyroid are positively correlated and serum free T_4 (fT_4) levels in cognitively normal individuals are negatively correlated with cerebral amyloid-β (Aβ) loads (*22*, *23*). These findings support the idea that modest dysregulation of THs can influence the development of AD. Moreover, T_3 levels in the prefrontal cortex are reduced in postmortem brains of patients with AD compared to controls, and T_3 and T_4 levels are also reduced in the cerebrospinal fluid of patients with AD (*24*). Given preclinical research on the involvement of THs in neurophenotypes and AD, TH deficiency could be linked to AD pathology, including amyloid plaques and neurofibrillary tangles. However, the mechanisms by which TH deficiency leads to AD pathological changes are unknown at the molecular level.

In this study, we found a correlation between decreased iodothyronine deiodinase 2 (DIO2) and TH deficiency in the brains of early AD model mice, indicating that early AD pathology reduces the conversion into active TH to restrict local availability of T_3 in the brain. TH deficiency led to spontaneous activation and reduced innate immune responses of microglia, which manifests as a failure to function properly or respond to pathogenic stimuli in the brain—one of the cardinal features of AD (*25*). Last, we defined a molecular mechanism in which TH-mediated microglial responsiveness was regulated by ecto-5′-nucleotidase (CD73) encoded by T_3-responsive *Nt5e* gene. This study reveals a requirement of THs for microglial functions to alleviate AD pathology and suggests a perspective on effective TH replacement therapy for patients with AD.

RESULTS

Decreased DIO2 is associated with hippocampal hypothyroidism in early AD model mice

We first sought to determine whether TH levels were changed in the blood and brains of early AD model mice before the development of widespread amyloid and tau pathologies. We measured TSH, fT_4, and fT_3 levels in the blood and brains of 4-month-old $ADLP^{APT}$

[1]Department of Biomedical Science, College of Medicine, Seoul National University, Seoul, Korea. [2]Convergence Dementia Research Center, College of Medicine, Seoul National University, Seoul, Korea. [3]Genomic Medicine Institute, Medical Research Center, Seoul National University, Seoul, Korea. [4]Center for Neuroscience, Brain Science Institute, Korea Institute of Science and Technology, Seoul, Korea.
*Corresponding author. Email: inhee@snu.ac.kr
†These authors contributed equally to this work.

(Alzheimer's disease-like pathology with APP, PSEN1, and MAPT) mice. All THs levels in the blood did not differ between 4-month-old ADLP^{WT} (wild-type) and ADLP^{APT} mice, but fT_4 levels were decreased in 7-month-old ADLP^{APT} mice (Fig. 1, A to C). Notably, hippocampal fT_3 levels were significantly decreased in ADLP^{APT} mice compared with ADLP^{WT} mice (Fig. 1D). Universal T_3-responsive gene expression, such as Hairless (*Hr*) and Krüppel-like factor 9 (*Klf9*) (*26*, *27*), was also decreased in the hippocampus of 4-month-old ADLP^{APT} mice with low hippocampal fT_3 (Fig. 1, E and F). However, fT_3, *Hr* mRNA, and *Klf9* mRNA levels were not changed in other brain regions, including the cortex, diencephalon, and midbrain (fig. S1, A to I).

To establish the cause of reduced hippocampal fT_3 in early AD model mice, we examined two possible systems that control TH homeostasis at the tissue level. First, intracellular TH levels are controlled by several TH converting enzymes including DIO2 and DIO3, involved in TH metabolism (*28*). In cases where the action of TH is required, cells preferentially take up circulating inactive T_4

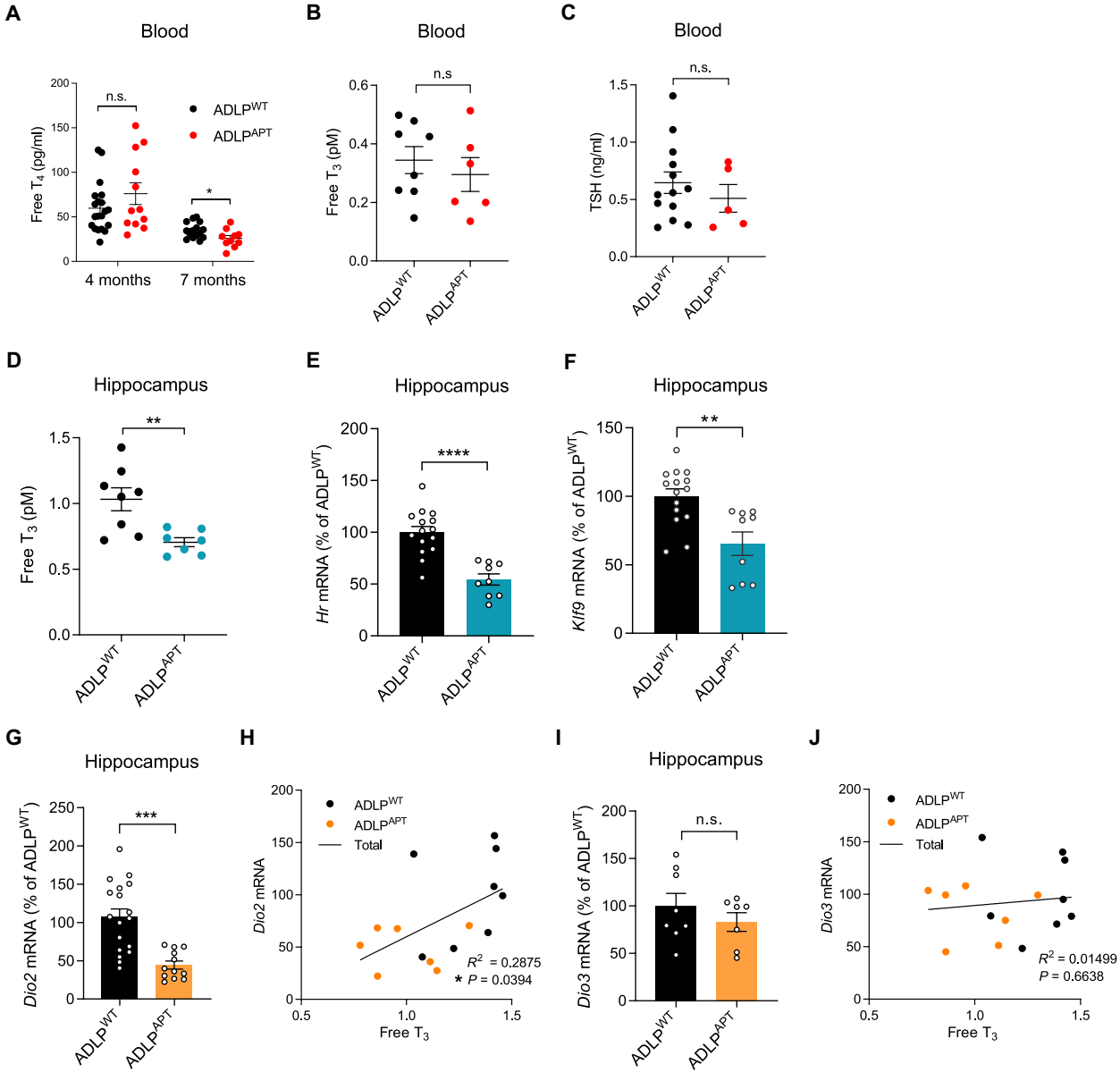

Fig. 1. Hippocampal TH deficiency develops in early AD model mice. (**A** to **C**) Serum fT_4 (A), fT_3 (B), and TSH (C) levels in 4-month-old ADLP^{WT} ($n = 20$) and ADLP^{APT} mice ($n = 12$). (**D**) Tissue fT_3 levels in the hippocampus of 4-month-old ADLP^{WT} ($n = 8$) and ADLP^{APT} mice ($n = 7$). (**E** and **F**) Expression of hippocampal TH-responsive gene transcript (*Hr* and *Klf9*) in 4-month-old ADLP^{WT} ($n = 15$) and ADLP^{APT} mice ($n = 9$). (**G**) Expression of hippocampal *Dio2* transcript in 4-month-old ADLP^{WT} ($n = 18$) and ADLP^{APT} mice ($n = 12$). (**H**) Correlation of *Dio2* transcript levels with hippocampal fT_3 levels in 4-month-old ADLP^{WT} ($n = 8$) and ADLP^{APT} mice ($n = 7$). Pearson correlation. (**I**) Expression of hippocampal *Dio3* transcript in 4-month-old ADLP^{WT} ($n = 8$) and ADLP^{APT} mice ($n = 7$). (**J**) Correlation of *Dio3* transcript levels with hippocampal fT_3 levels in 4-month-old ADLP^{WT} ($n = 8$) and ADLP^{APT} mice ($n = 7$). Pearson correlation. Data represent means ± SEM. R^2 = coefficient of determination. In (A) to (G) and (I), *P* values were calculated using two-tailed unpaired *t* test. $^*P < 0.05$, $^{**}P < 0.01$, $^{***}P < 0.001$, and $^{****}P < 0.0001$. n.s., not significant.

and convert it to active T_3 through the action of deiodinases (*29*). DIO2 plays a role in providing active T_3 in the central nervous system, whereas DIO3 terminates TH activity through deiodination of the tyrosyl ring (*30*). Hippocampal *Dio2* was reduced in 4-month-old ADLP^{APT} mice (Fig. 1G) and positively correlated with hippocampal fT_3 levels (Fig. 1H). In contrast, hippocampal *Dio3* was not significantly different between ADLP^{WT} and ADLP^{APT} mice, and hippocampal fT_3 levels were not correlated with hippocampal *Dio3* levels (Fig. 1, I and J). In addition, cortical *Dio2* was decreased, but no alterations were detected in other brain regions (fig. S1, J to L). The other system influencing T_3 availability at the tissue level is TH transporters, which are differentially expressed among various tissues (*31*). Hippocampal expression of the TH transporters, *Slc7a5*, *Slc7a8*, *Slc16a2*, *Slc16a10*, *Slco1c1*, and *Slco2b1*, did not differ between ADLP^{WT} and ADLP^{APT} mice, suggesting that TH transport may therefore be intact in early AD model mice (fig. S2).

Similar to the phenotypes in ADLP^{APT} mice, hippocampal *Dio2* was also reduced early in different AD model mice that develop either amyloid or tau pathology (fig. S3A). Human sporadic AD (sAD) and familiar AD (fAD) organoids showing amyloid and tau pathology showed reduced DIO2 (fig. S3, B to F). fAD brain organoids exhibiting more distinct AD pathological symptoms than sAD brain organoids showed a significant decrease in DIO2 expression compared to sAD brain organoids, suggesting that reduced DIO2 is associated with AD pathological symptoms. Reduced DIO2 in fAD brain organoids led to down-regulation of TH-related pathways following T_4 treatment (fig. S3G). Last, DIO2 immunoreactivity was decreased in the hippocampus of human postmortem AD brains (fig. S3, H and I, and table S2). These data are consistent with our findings of reduced DIO2 in the hippocampus of AD model mice.

To further investigate the distinction of local hypothyroidism in the hippocampus, we analyzed DIO2 protein in the hippocampus and cortex. We found a reduction in hippocampal DIO2, whereas cortical DIO2 remained changed, despite a reduction in cortical *Dio2* (fig. S4, A and B). With the pathological progression, both hippocampal *Dio2* mRNA and DIO2 protein were significantly reduced in 7-month-old AD model mice compared with 4-month-old mice, but cortical DIO2 expression was not altered in 7-month-old AD model mice (fig. S4, C to E), suggesting hippocampal susceptibility of DIO2 expression to AD pathology. In addition, we analyzed *DIO2* expression associated with human AD pathology and clinical symptoms using the human brain transcriptome database (Allen Institute for Brain Science: Aging, dementia, and TBI study). Similar to the reduction in hippocampal *Dio2* in AD model mice, hippocampal *DIO2* was more significantly associated with both the pathological progression and clinical phenotypes of dementia than cortical *DIO2* in the parietal and temporal cortex (fig. S4, F and G). In summary, our data suggest that local hippocampal hypothyroidism is associated with decreased DIO2 expression by AD pathology.

TH deficiency leads to impaired innate immune responses in microglia

To determine the effect of TH deficiency on the brain, we performed single-cell RNA sequencing (scRNA-seq) of the hippocampus in AD model mice fed an iodine-deficient (ID) diet for 10 weeks, which completely depleted fT_4 levels in the blood (Fig. 2A). A total of 6502 single cells were sequenced. Clustering analyses revealed 11 populations in each cluster based on cell type–specific marker genes. The cell population we identified mainly consisted of glial cells, namely, oligodendrocytes, oligodendrocyte precursor cells, and microglia (fig. S5A). Among the identified cell populations, only the microglial population showed significant alterations by the ID diet (fig. S5B), as reported previously (*32*). The observed changes in microglial density in the hippocampus were further confirmed by counting the number of Iba1$^+$ cells and measuring Iba1 staining intensity (fig. S5, C to E). Given that THs regulate various microglial functions, including migration and phagocytosis (*33*), we next sought to determine the impact of TH deficiency on microglial immune activity. Gene Ontology pathway analysis of differentially expressed genes (DEGs) revealed the up-regulation of inflammation-associated pathways in ADLP^{WT} mice fed the ID diet, despite the absence of AD pathology (Fig. 2B). Pathways such as "positive regulation of extracellular signal–regulated kinase 1 (ERK1) and ERK2 cascade" and "positive regulation of nitric oxide biosynthetic process" indicative of activated microglia were increased by the ID diet (*34*–*36*). Microglial activation signatures induced by the ID diet included up-regulation of genes including *Il1b*, *Tnfa*, and multiple chemokines (Fig. 2C). Proinflammatory genes (*Il1b*, *Tnfa*, *Ccl6*, *C1qa*, *Cd83*, *Abca1*, and *Ccr6*) and anti-inflammatory cytokine genes (*Il4* and *Il10*) up-regulated in the hippocampus of ADLP^{WT} mice fed the ID diet were validated by quantitative polymerase chain reaction (qPCR) (Fig. 2D).

Next, we examined microglial responsiveness modulated by TH. Using two-photon microscopy, in vivo imaging revealed reduced responsiveness toward acute laser-induced tissue damage in *Cx3cr1*$^{gfp/+}$ mice fed the ID diet (Fig. 2, E and F, and movies S1 and S2). In the absence of THs, microglia spontaneously expressed higher levels of proinflammatory (*Il1b* and *Tnfa*) and anti-inflammatory (*Il4* and *Il10*) cytokines under nonstimulated conditions (Fig. 2G), indicating their constitutively activated status, consistent with the in vivo observations (Fig. 2, B and C). However, upon lipopolysaccharide (LPS) or oligomer Aβ treatment, microglia produced fewer proinflammatory cytokines with no change in anti-inflammatory cytokines. These findings suggest that the spontaneous activation of microglia caused by TH deficiency does not adequately provoke immune responses to inflammatory stimuli (Fig. 2, H and I, and fig. S6, A and B). To determine whether compromised microglial functions in the absence of THs are attributed to changes in metabolic efficiency or signaling pathways of external stimuli, we analyzed metabolic-related signaling pathways activated by immune stimuli in microglia through Western blot analysis (*25*). Metabolism-related signaling pathways were normally altered by LPS, independent of TH (fig. S6, C and D). These data suggest that impaired microglial innate immune responses caused by TH deficiency occur independently of changes in metabolic efficiency. Together, TH deficiency causes the spontaneous activation of microglia, and TH is required to prime microglia for appropriate immune responses to external stimuli.

TH deficiency aggravates amyloid pathology

To determine whether TH deficiency affects AD pathologies in the hippocampus, we fed ADLP^{APT} mice exhibiting both amyloid and tau pathology the ID diet for 10 weeks, which completely depleted fT_4 levels in the blood (Fig. 3A). TH deficiency increased levels of both $A\beta_{40}$ and $A\beta_{42}$ in radioimmunoprecipitation assay (RIPA)–insoluble fractions containing amyloid plaques in the hippocampus, as measured by enzyme-linked immunosorbent assays (ELISAs) (Fig. 3B). We next performed immunohistochemistry for amyloid

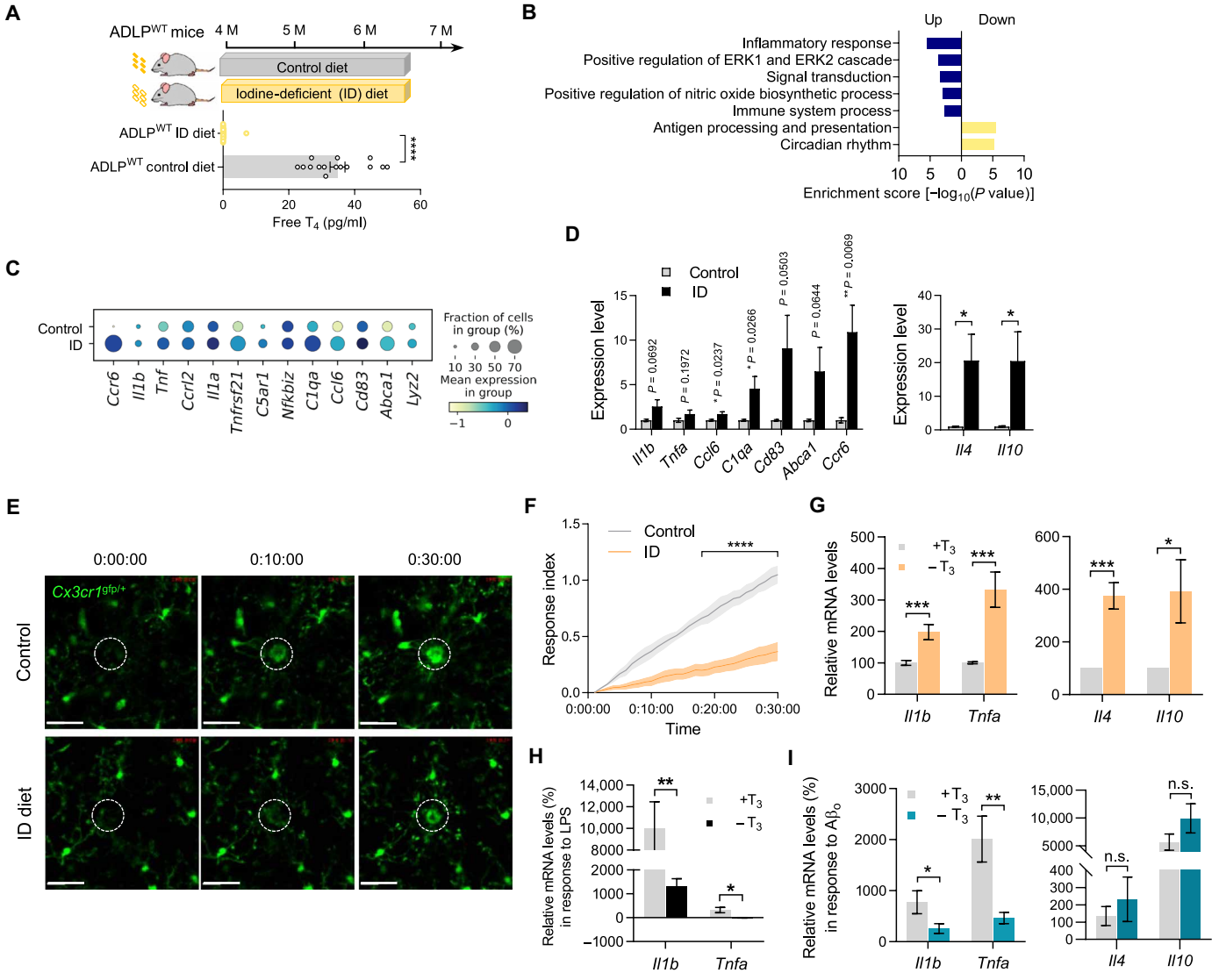

Fig. 2. TH deficiency induces spontaneous activation of microglia, resulting in suppressed innate immune response. (**A**) Scheme for inducing TH deficiency and measuring serum fT_4 ($n = 15$ per group). (**B**) Gene Ontology analysis of microglial DEGs in the ID group. (**C**) Heatmap showing expression of inflammation-associated microglial genes. (**D**) Expression of inflammation-associated genes and anti-inflammatory cytokines transcript in the hippocampus by qPCR. (**E**) Representative in vivo microglial responses, imaged by two-photon microscopy. Shown are 7-month-old *Cx3cr1*$^{gfp/+}$ mice after induction of TH deficiency for 10 weeks. The white circle denotes the site of laser damage. Scale bars, 50 μm. (**F**) Quantification of microglial recruitment toward the damaged site. (**G**) Expression of pro- (*Il1b* and *Tnfa*) and anti-inflammatory (*Il4* and *Il10*) cytokine transcript in primary microglia treated with or without T_3. (**H**) Expression of *Il1b* and *Tnfa* transcript in LPS-pretreated primary microglia treated with or without T_3. (**I**) Expression of *Il1b*, *Tnfa*, *Il4*, and *Il10* transcript in oligomer Aβ-pretreated primary microglia treated with or without T_3. Data represent means ± SEM. In (G) to (I), *P* values were calculated using two-tailed unpaired *t* test. $*P < 0.05$, $**P < 0.01$, $***P < 0.001$, and $****P < 0.0001$.

plaques in the hippocampus using anti-Aβ antibody (4G8), which showed that the ID diet increased the area and intensity of amyloid plaques (Fig. 3, C and D). The total number of amyloid plaques, as well as those categorized by diameter, also increased (Fig. 3, E and F). Higher plaque burdens were associated with a faster cognitive decline in AD model mice fed the ID diet (Fig. 3G). To further examine whether TH deficiency induces Aβ generation, we examined amyloidogenic processing. Analysis of RIPA-soluble fractions of $Aβ_{40}$ and $Aβ_{42}$ showed no effect of the ID diet on the generation of soluble Aβ in the hippocampus (Fig. 3H). Moreover, the levels of full-length human amyloid precursor protein (APP) and cleaved soluble APP-β were not altered by the ID diet in the hippocampus of ADLP^{APT} mice (Fig. 3, I and J), suggesting no changes in APP expression and processing. In addition to amyloid pathology, we investigated tau pathology in the hippocampus of ADLP^{APT} mice fed the control or ID diet. In contrast to amyloid pathology, TH deficiency had no significant effect on phosphorylated tau or aggregated tau levels in the hippocampus (fig. S7). Together, our findings suggest that TH deficiency accelerates the progression of amyloid pathology and memory impairments.

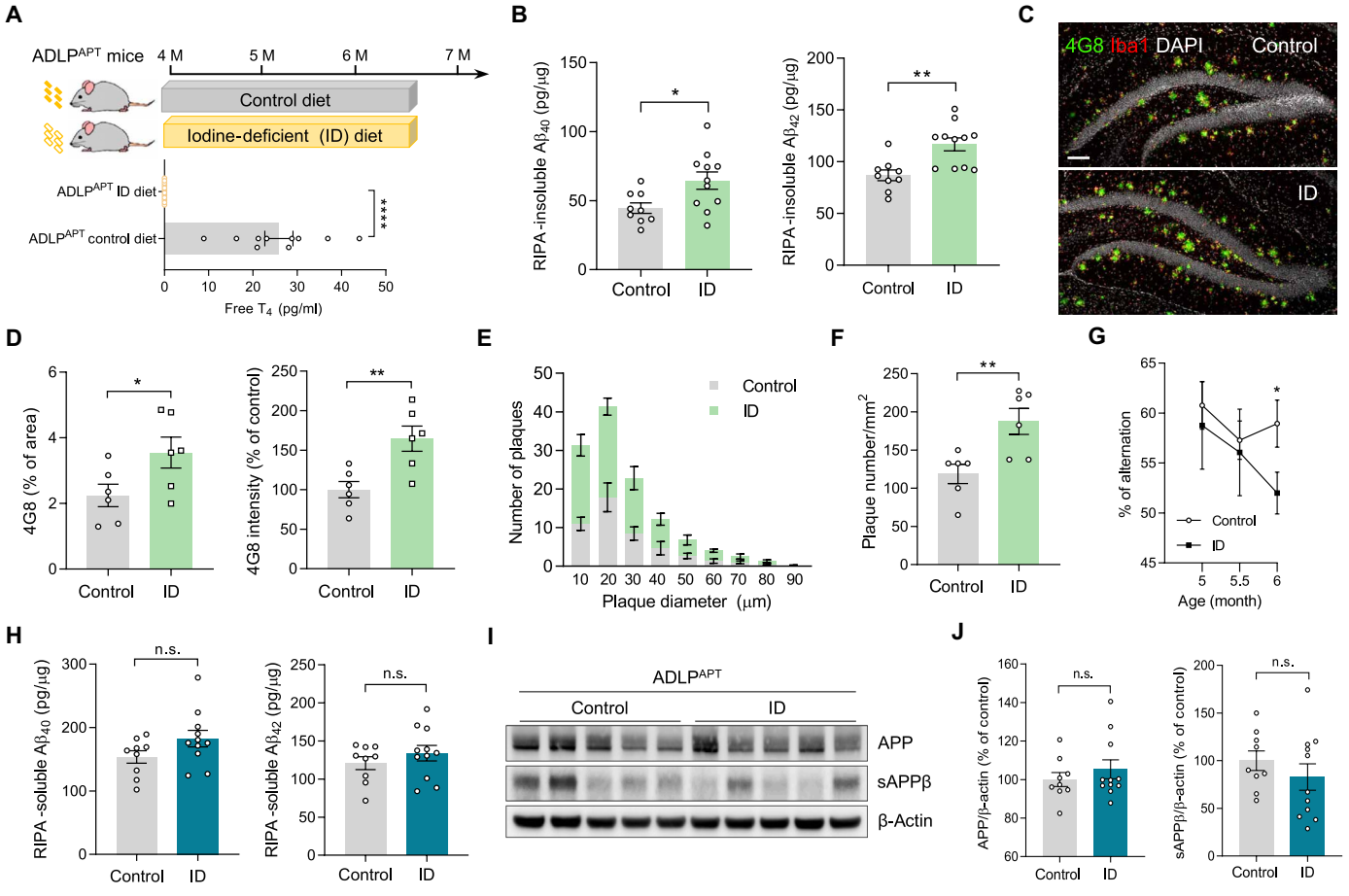

Fig. 3. TH deficiency aggravates amyloid pathology. (**A**) Scheme for inducing TH deficiency and measuring serum fT_4 in $ADLP^{APT}$ mice (control, $n = 9$; ID diet, $n = 11$). (**B**) Measurement of $A\beta_{40}$ and $A\beta_{42}$ in the RIPA-insoluble fraction from the hippocampus, assessed by ELISA (control, $n = 9$; ID diet, $n = 11$). (**C**) Representative images of amyloid plaques (4G8) and $Iba1^+$ microglia in the hippocampus of $ADLP^{APT}$ mice fed the control or ID diet. DAPI, 4′,6-diamidino-2-phenylindole. Scale bar, 100 μm. (**D**) Quantification of 4G8 signals ($n = 6$ per group). (**E**) Distribution of plaque size in the hippocampus of mice from control and ID diet groups. (**F**) Quantification of plaque numbers in the hippocampus of mice in control and ID diet groups ($n = 6$ per group). (**G**) Percentage of alternations in a Y-maze task (control, $n = 11$; ID diet, $n = 12$). (**H**) Measurement of $A\beta_{40}$ and $A\beta_{42}$ in the RIPA-soluble fraction from the hippocampus, assessed by ELISA (control, $n = 9$; ID diet, $n = 11$). (**I** and **J**) Representative immunoblots (I) and quantification (J) of APP and soluble APPβ, as a measure of amyloidogenic processing (control, $n = 9$; ID diet, $n = 11$). Data represent means ± s.e.m. In (B), (D), (F), (G), (H), and (J), *P* values were calculated using two-tailed unpaired *t* test. $*P < 0.05$, $**P < 0.01$, and $****P < 0.0001$.

TH deficiency decreases disease-associated microglia in AD model mice

Given the effect of TH deficiency on microglia in the brain (Fig. 2 and fig. S5) and the role of microglia in amyloid clearance (*37*, *38*), we next investigated whether TH deficiency caused microglial changes in AD model mice. To characterize changes in microglial subpopulations induced by TH deficiency, we compared microglial single-cell data from $ADLP^{APT}$ mice fed either the control or ID diet. Cluster analysis based on single-cell level transcriptional profiles of microglia revealed seven distinct microglial states across all diet conditions (control or ID diet) and genotypes ($ADLP^{WT}$ or $ADLP^{APT}$ mice) (Fig. 4A). These distinct microglial subpopulations were characterized on the basis of cluster-specific transcriptomes, mitochondrial gene ratios, and the number of detected genes (figs. S8 and S9). We determined the pseudotime trajectory of microglial activation from homeostatic microglia toward degenerating disease-associated microglia (DAM) in AD model mice, produced using Monocle single-cell trajectory analysis (Fig. 4B). Examination of the percentage of microglial subpopulations revealed that the ID diet induced an increase in cluster 0 (activated) and cluster 5 (interferon-responsive) but a marked reduction in cluster 2 (DAM) (Fig. 4C). We confirmed that TH deficiency led to a decrease in DAM signature gene expression by scRNA-seq and qPCR, supporting a decreased DAM population (Fig. 4D).

Given the protective role of DAM, with potent phagocytic activity, in restricting neurodegeneration (*39*, *40*), we next defined the impact of TH deficiency on microglial phagocytosis in AD model mice. Although the quantification of Iba1 immunofluorescence intensity and the percentage area showed no difference in microglial activation between the two groups, we found that microglia were not activated well, considering the increase in amyloid plaques in the ID group (Fig. 4, F to I). The number of phagocytic microglia with 4G8-positive signals around amyloid plaques was significantly

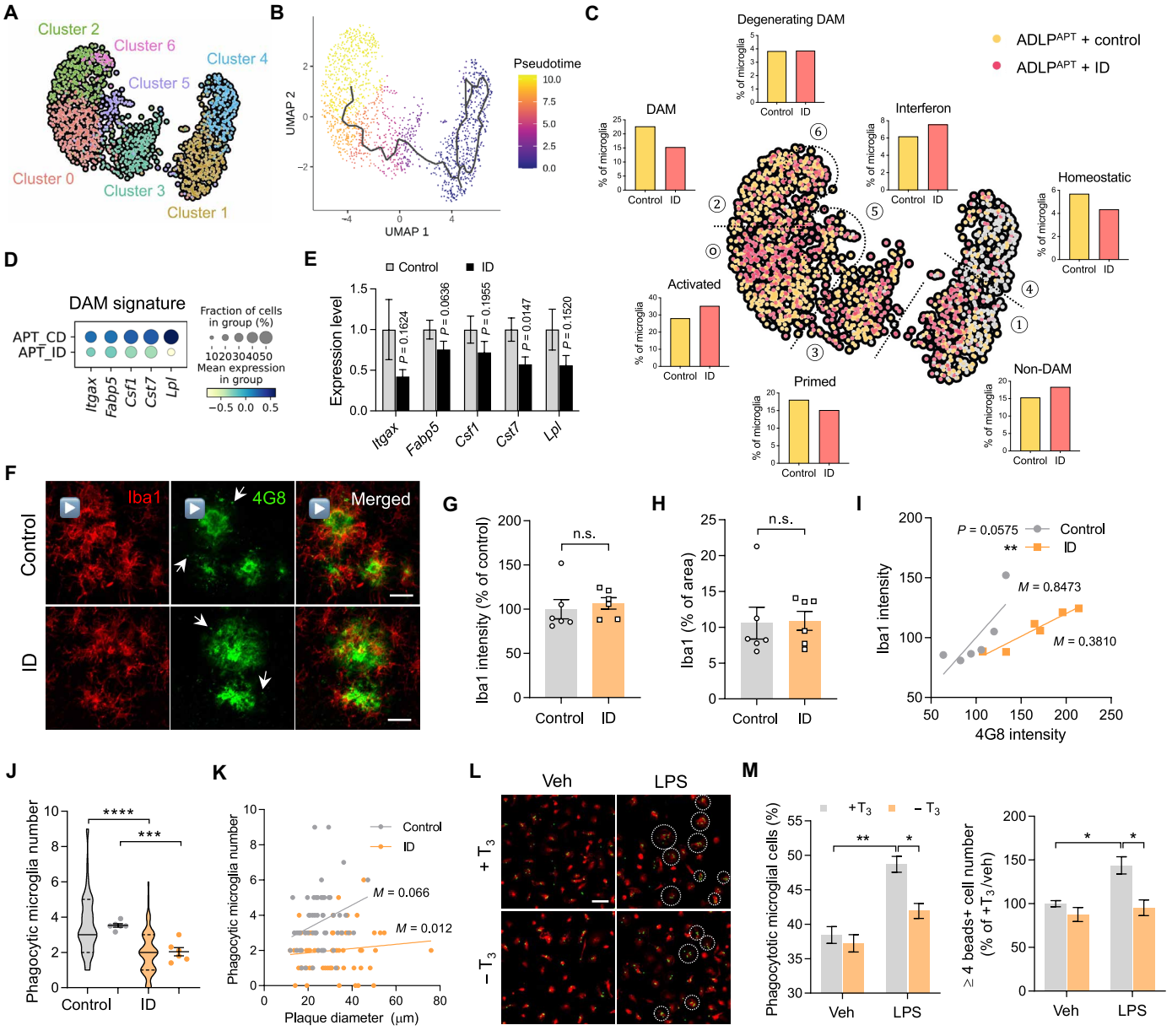

Fig. 4. TH deficiency suppresses phagocytic activity of microglia in AD model mice. (**A**) Uniform Manifold Approximation and Projection (UMAP) plot of seven microglial subsets. (**B**) Monocle trajectory analysis depicting pseudotime trajectories of microglial subsets. (**C**) UMAP plot and the percentage of each microglia subset in ADLP^{APT} mice, annotated according to diet. (**D**) Heatmap showing expression of DAM signature genes in microglia. (**E**) Expression of DAM signature gene transcripts in the hippocampus by qPCR. (**F**) Representative images of Iba1^{+} microglia around amyloid plaques (4G8) in the hippocampus of ADLP^{APT} mice fed a control or ID diet (arrows, phagocytic microglia; arrowheads, barrier of microglia). Scale bars, 20 μm. (**G** and **H**) Quantification of Iba1 signals ($n = 6$ per group). (**I**) Correlation of Iba1 intensity and 4G8 intensity [Pearson correlation (M) = slope]. (**J**) Violin plots showing the number of phagocytic microglia per amyloid plaque. Colored dots to the right of violin plots indicate means per individual mouse. (**K**) Correlation of phagocytic microglia number and plaque diameter [Pearson correlation (M) = slope]. (**L**) Representative images of bead-uptake assays following the treatment of primary microglia with T_3 and/or LPS. White circles indicate phagocytic microglia containing more than four beads. (**M**) Quantification of phagocytic microglia. Data represent means ± SEM. In (G), (H), and (J), P values were calculated using two-tailed unpaired t test. In (M), P values were calculated using two-way analysis of variance (ANOVA). *$P < 0.05$, **$P < 0.01$, ***$P < 0.001$, and ****$P < 0.0001$.

lower in the ID group despite their larger amyloid plaque size (Fig. 4, J and K). The low phagocytic activity of microglia caused by TH deficiency was also validated by in vitro bead-uptake assays (Fig. 4, L and M). Together, our data suggest that TH deficiency increases amyloid pathology by reducing DAM population and limiting amyloid clearance in microglia.

T_3 administration alleviates microgliosis and AD pathology

Since the conversion of T_4 to T_3 in the brains of ADLP^{APT} mice was impaired because of decreased DIO2, we assessed whether providing additional THs would alleviate AD pathology by administering converted active T_3 to ADLP^{APT} mice. Following daily intraperitoneal injection of T_3 for 8 weeks, we confirmed the up-regulation of

universal T_3-responsive genes in the hippocampus (fig. S10, A and B). We next isolated sarkosyl-soluble and -insoluble tau from the hippocampus of ADLP^{APT} mice. T_3 administration significantly reduced sarkosyl-insoluble, -soluble, and phosphorylated tau in the hippocampus of ADLP^{APT} mice (fig. S10, C and D). Decreases in phosphorylated tau (AT180) and total human tau in the hippocampus of T_3-injected ADLP^{APT} mice were confirmed by immunohistochemistry (fig. S10E). In addition to tau pathology, T_3 injection alleviated amyloid plaque formation in the hippocampus of ADLP^{APT} mice (fig. S10F). Furthermore, mitigation of AD pathology through T_3 supplementation rescued memory impairment in ADLP^{APT} mice (fig. S10G).

Next, we analyzed whether T_3 administration mitigated AD-related gliosis in the hippocampus. Notably, microglial activation (Iba1$^+$ microglia) was significantly reduced in ADLP^{APT} mice with T_3 administration, whereas astrocytic activation (glial fibrillary acidic protein–positive astrocytes) remained unchanged (fig. S11, A to C). A significant decrease in the area immunoreactive for both Iba1 and CD68, a lysosomal protein expressed in macrophages and activated microglia (*41*), was observed in the hippocampus of T_3-injected ADLP^{APT} mice (fig. S11, D and E). These results suggest that T_3 supplementation ameliorates AD-associated brain pathologies in ADLP^{APT} mice and alleviates brain lesions, predominantly by modulating microglial activation.

CD73 expression is regulated in a TH-dependent manner and is required for innate immune responses of microglia

To determine potential molecular mediators of TH-regulated microglial functions, we performed bulk RNA-seq of primary microglia treated with or without T_3. While we found DEGs in scRNA-seq analyses of the hippocampus because of sequencing depth across single cells, most microglial DEGs were highly expressed genes associated with inflammatory response phenotypes. The TH-dependent transcriptional profiling indicated that up-regulated DEGs predominated over down-regulated genes following T_3 treatment, suggesting the role of T_3 as a transcriptional activator (Fig. 5A). Notably, the most up-regulated T_3-induced DEG in primary microglia, as determined by Gene Set Enrichment Analysis Singal2Noise (GSEA S2N) analysis, was CD73 (Fig. 5B), an ecto-5′-nucleotidase known for inducing immunosuppression through the conversion of adenosine monophosphate to adenosine, binding to adenosine receptors on immune cells (*42*, *43*). The role of CD73 as an inhibitory immune checkpoint has been explored in the context of cancer cells escaping immune surveillance in the tumor microenvironment (*44*, *45*). Previous studies have reported that TH up-regulates CD73 expression in different cell types (*46*–*48*). Microglia without T_3 expressed lower levels of CD73 at both mRNA and protein levels (Fig. 5, C and D). Moreover, CD73 was transcriptionally up-regulated by T_3 in a concentration-dependent manner, indicating that *Nt5e*, which encodes CD73, is a TH-responsive gene (Fig. 5E). In line with the regulation of CD73 expression in vitro, CD73 protein levels were reduced in the hippocampus by the ID diet (Fig. 5F). In AD model mice, microglia sorted by magnetic-activated cell sorting showed decreased levels of CD73(*Nt5e*) mRNA but no alteration in their nonmicroglial cell population (Fig. 5G), supporting the conclusion that microglia were predominantly affected by the ID diet and T_3 administration in vivo.

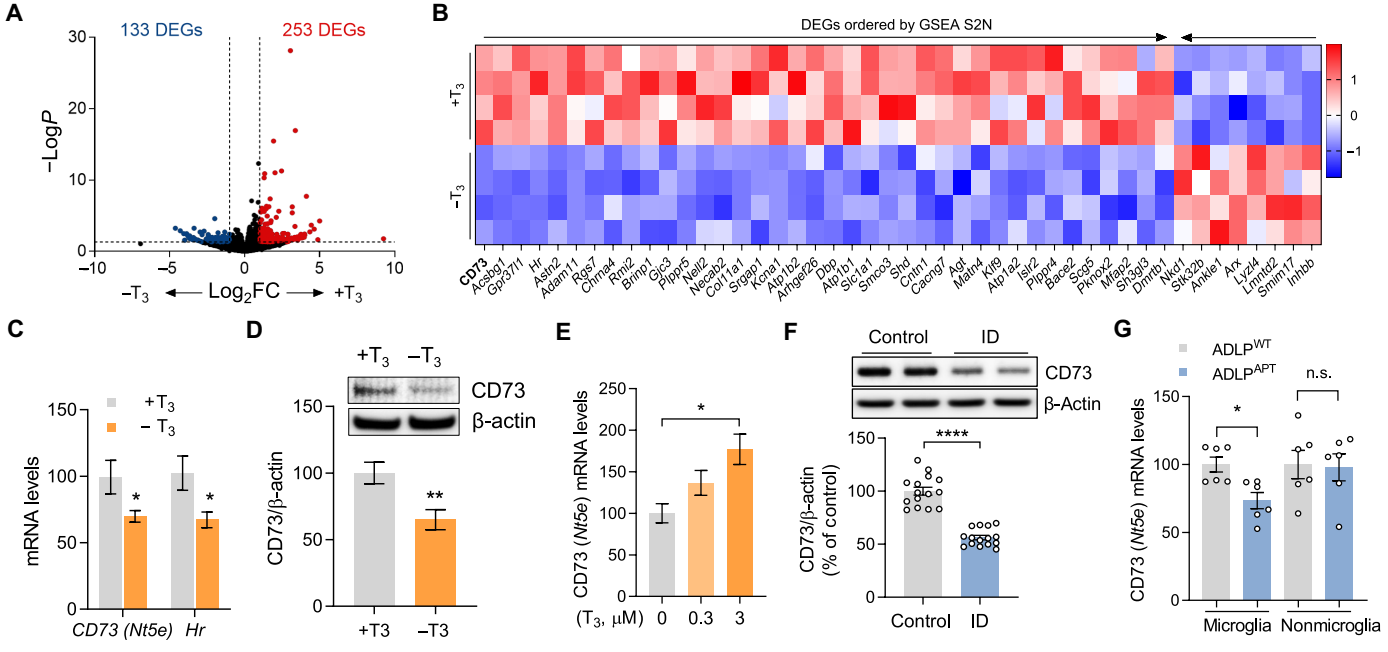

Fig. 5. TH-dependent regulation of CD73 expression in microglia. (**A**) Volcano plot of microglial DEGs following T_3 treatment. FC, fold change. (**B**) Heatmap of microglial DEGs ordered using GSEA S2N. (**C**) Expression of CD73 (*Nt5e*) and *Hr* transcript in primary microglia treated in the absence of T_3. (**D**) Representative immunoblots and quantification of CD73 in primary microglia in the absence of T_3. (**E**) Expression of CD73 (*Nt5e*) transcript in primary microglia following T_3 treatment. (**F**) Representative immunoblots and quantification of CD73 in the hippocampus of wild-type mice fed the ID diet ($n = 15$ per group). (**G**) Expression of CD73 (*Nt5e*) transcript in microglia and nonmicroglial populations from the hippocampus of wild-type and ADLP^{APT} mice ($n = 6$ per group). Data represent means ± SEM. *P* values were calculated using two-tailed unpaired *t* test. In (E), *P* values were calculated using one-way ANOVA. $^*P < 0.05$, $^{**}P < 0.01$, and $^{****}P < 0.0001$.

To assess whether the inhibition of CD73 blocks microglial immune responses to inflammatory stimuli, we pretreated microglia with the CD73 inhibitor, adenosine 5′-(α,β-methylene)diphosphate sodium salt (AMPCP) before LPS treatment. Similar to the effects of TH deficiency on microglial immune responses (Fig. 2, H and I), AMPCP reduced proinflammatory cytokine gene expression in CD73-inhibited microglia following LPS treatment (Fig. 6A). Using two-photon microscopy, we also observed reduced microglial motility toward acute tissue damage insults in vivo following AMPCP intraperitoneal administration (Fig. 6, B and C, and movies S3 and S4). We next examined the role of CD73 in amyloid pathology in ADLP$^{APP/PS1}$ mice after AMPCP intraperitoneal administration for 8 weeks. Amyloid plaque burdens were increased in the hippocampus of the AMPCP-injected group (Fig. 6, D and E). Given the increased amyloid pathology by AMPCP, microglia were relatively less activated in the hippocampus (Fig. 6F). In addition, similar to the decreased DAM signature gene expression in microglia of the ID diet group (Fig. 4, D and E), overall DAM-related gene expression was reduced in the hippocampus of AMPCP-injected mice, as assessed by qPCR (Fig. 6G). Using live-cell imaging, we performed a phagocytosis assay with primary microglia for pHrodo Red–labeled oligomer Aβ, which turns red fluorescence in an acidic environment of the lysosome. After 24 hours of live-cell imaging following the treatment of pHrodo Red–labeled oligomer Aβ with either vehicle

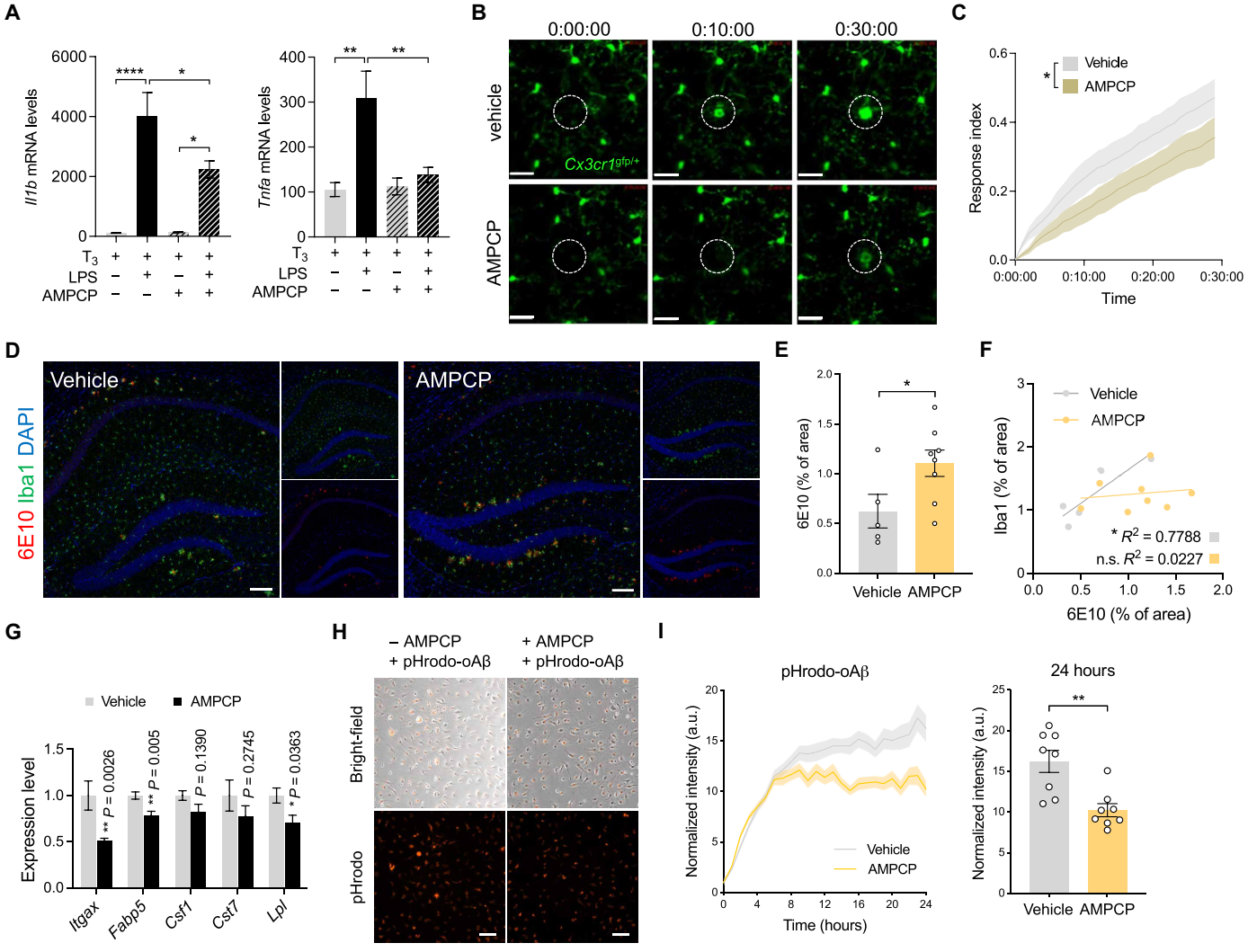

Fig. 6. CD73 inhibition suppresses innate immune responses of microglia to inflammatory stimuli and AD pathology. (**A**) Expression of *Il1b* and *Tnfa* transcript in primary microglia following T_3, LPS, and/or AMPCP treatment. (**B**) Representative in vivo microglial responses after AMPCP administration, imaged by two-photon microscopy. Shown are 6-month-old *Cx3cr1*$^{gfp/+}$ mice after AMPCP administration for 4 weeks. The white circle denotes the site of laser damage. Scale bars, 25 μm. (**C**) Quantification of microglial recruitment toward the damaged site. (**D**) Representative images of amyloid plaques (6E10) and Iba1$^+$ microglia in the hippocampus of ADLP$^{APP/PS1}$ mice injected with vehicle or AMPCP. Scale bars, 100 μm. (**E**) Quantification of 6E10 signals (vehicle, $n = 5$; AMPCP, $n = 8$). (**F**) Correlation of Iba1 intensity and 6E10 intensity. (**G**) Expression of DAM signature gene transcripts in the hippocampus by qPCR. (**H**) Representative images of phagocytosis assays following the treatment of primary microglia with pHrodo Red–oAβ and/or AMPCP. White circles indicate phagocytic microglia containing more than four beads. Scale bars, 100 μm. (**I**) Quantification of normalized intensity of pHrodo Red at 24-hour time point of live-cell imaging. a.u., arbitrary units. Data represent means ± SEM. *P* values were calculated using two-tailed unpaired *t* test. In (A), *P* values were calculated using two-way ANOVA. $^*P < 0.05$, $^{**}P < 0.01$, and $^{****}P < 0.0001$.

or AMPCP, we observed a significant decrease in phagocytic activity in microglia of the AMPCP-treated group (Fig. 6, H and I). Together, we found that TH transcriptionally modulated microglial CD73, acting as an inhibitory immune checkpoint that ensures proper immune responses to inflammatory stimuli, including Aβ in AD.

DISCUSSION

Here, we established that TH deficiency suppresses innate immune responses in microglia, resulting in aggravation of AD pathology. We found that brain hypothyroidism occurs in the hippocampus of early AD model mice before it manifests in the blood. Notably, the decrease in the local conversion of inactive T_4 to active T_3 was first detected in the hippocampus of early AD model mice and was closely correlated with decreased DIO2. Last, we revealed that TH deficiency significantly reduces the DAM population and elucidated a TH-mediated mechanism that modulates microglial activity via CD73, a TH-responsive gene product.

Our study of TH homeostasis at the tissue level gives support for local hypothyroidism in AD. First, we demonstrated that TSH, fT_3, and fT_4 levels, used to diagnose clinical hypothyroidism (*49*), are unaffected in the blood, whereas tissue fT_3 levels are reduced in the brain beginning in the early stages of AD model mice. Among the various brain regions, the hippocampus first showed a considerable decrease in fT_3 levels and TH-responsive gene expression, suggesting a link between brain region–specific hypothyroidism, particularly in the hippocampus, and AD. Given that structural heterogeneity and tissue weight vary across brain regions, TH measurement with dissected brain subregions would be possible to precisely define regional hypothyroidism in each for further study. Second, down-regulation of TH conversion to its active form shows altered TH metabolism in the AD brains. Decreased fT_3 levels were specifically correlated to *Dio2*, which converts T_4 to T_3, not to other deiodinases, TH degradation, transporters, or receptors expression. Reduced hippocampal DIO2 observed in early AD model mice, unlike cortical DIO2, also decreased as AD pathology progressed. Inactivation of DIO2 by a common polymorphism ($Thr^{92}Ala$), which is susceptible to ubiquitination and degradation, has been linked to tissue-specific hypothyroidism (*50*, *51*). However, we found that a reduction in DIO2 in the AD brains was attributable to transcriptional down-regulation. Further research will be required to understand the underlying molecular processes by which DIO2 is down-regulated in the AD brains.

TH deficiency has a substantial effect on the microglial population in the brain. In the context of TH deficiency, our single-cell dataset demonstrated that microglia in wild-type mice exhibit spontaneous activation states and subsequently reduced immune responses to external stimuli. Previous research has found that TH plays a role in microglia development, morphological differentiation, and proliferation (*32*, *52*, *53*). A decrease in microglia density increases the brain area for which each microglial cell is responsible and may increase the external stimuli to which microglia are exposed, resulting in reduced innate immune responses. However, microglia in AD respond differently to TH deficiency. In cases when microgliosis has already developed because of amyloid pathology, TH deficiency is primarily responsible for lowering microglial immune function. Significantly, TH deficiency reduces DAM population and reduces phagocytic clearance of amyloid plaques. The decrease in DAM cluster, the population of phagocytic microglia, caused by TH deficiency leads to the growth of amyloid plaques. Thus, our findings suggest that THs are required for DAM development in the AD brains.

To explain the mechanism underlying reduced innate immune responses of microglia by TH deficiency, we investigated genomic actions of TH in microglia using bulk RNA-seq. CD73, the top-ranked DEG transcriptionally regulated by TH, functions as an inhibitory immune checkpoint by converting adenosine monophosphate to adenosine, which activates immune suppression via adenosine receptors (*54*). A recent study found that CD73, through supplying adenosine to neurons, exerts microglia-derived negative feedback on neuronal activity in the brain (*55*). Our findings showed that inhibiting CD73 phenocopies reduced immune responses in microglia caused by TH deficiency. Microglia with low CD73 levels due to TH deficiency are in an activated state because the lack of immunosuppressive adenosine spontaneously activates microglia even under nonstimulated conditions. Spontaneously activated microglia do not properly provoke innate immune responses to immune, damage, and disease insults. Reduced microglial CD73 caused by TH deficiency in early AD model mice results in the reduced innate immune responses that limit amyloid clearance by microglia.

In summary, our findings define a reciprocal relation between AD pathology and hypothyroidism, notably in the brain. Reduced DIO2 levels are associated with down-regulated TH pathways in the hippocampus at an early stage of AD model mice. TH deficiency in the brain has a substantial impact on microglia, leading to reduced immune responses in microglia and an aggravation of AD pathogenesis (Fig. 7). This suggests that THs play a critical role in the reciprocal link between microglia and AD pathogenesis. Understanding altered TH metabolism in the AD brains will lead to therapeutic strategies for AD while preserving microglial immune functions.

MATERIALS AND METHODS

The methods are described in detail in the Supplementary Materials.

Animals

5xFAD transgenic mice harboring mutated human APP ($APP^{K670N/M671L, I716V, V717I}$) and presenilin1 ($PSEN1^{M146l, L286V}$) were obtained from the Jackson laboratory (Tg6799, stock number 006554). JNPL3 transgenic mice harboring mutated human tau^{P301L} were obtained from Taconic (TauP301L-JNPL3, stock number 2508). For observations of both amyloid and neurofibrillary tangle pathologies, the two strains were crossed to generate ADLP transgenic mice, as previously described (*56*). Progeny with four genotypes—$ADLP^{WT}$, $ADLP^{APP/PS1}$, $ADLP^{Tau}$, and $ADLP^{APT}$—showing Aβ and/or tau pathologies were confirmed by PCR from ear clippings. Because AD pathologies are more rapidly exacerbated in female mice compared with male mice, only female ADLP transgenic mice were used in these studies. Transgenic mice expressing green fluorescent protein under control of the endogenous *Cx3cr1* locus ($Cx3cr1^{gfp/gfp}$ mice) were obtained from the Jackson laboratory (stock number 008451). These mice were crossed with C57BL/6, and their offspring ($Cx3cr1^{gfp/+}$ mice) were used for in vivo two-photon imaging of microglial morphology and function. All animals were maintained in a specific pathogen–free animal facility of Seoul National University and were housed under a 12/12-hour light-dark cycle with ad libitum access to food and water. All animal experimental procedures were carried out in accordance with the principles of Laboratory Animal Care

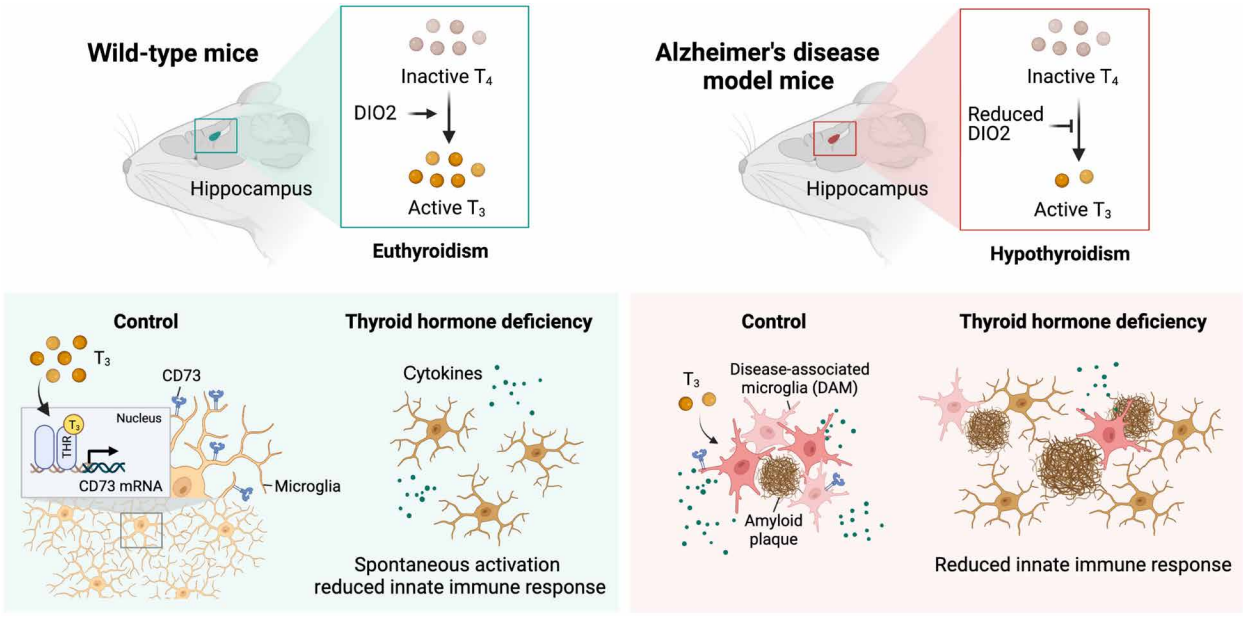

Fig. 7. Graphic summary. Scheme illustrating local hippocampal hypothyroidism caused by decreased DIO2 and its subsequent effect on microglial immune responses in AD model mice. The graphic summary was created with confirmation of publication and licensing rights from BioRender.com.

(National Institutes of Health publication no. 85-23, revised 1985) and the Animal Care and Use Guidelines of Seoul National University, Seoul, Korea.

Induction of hypothyroidism

Hypothyroidism was induced by feeding 16-week-old ADLP and *Cx3cr1*$^{gfp/+}$ mice an ID diet supplemented with 0.15% propylthiouracil (Envigo, TD.95125) for 10 weeks. Control euthyroid mice of the same age were fed a normal diet for 10 weeks.

T_3 and AMPCP injections

For T_3 administration in ADLP mice, 3,3′,5-triiodo-l-thyronine sodium salt (T_3; Sigma-Aldrich, T6397) was prepared at 50 mg/ml in 1 M NaOH and diluted in saline to obtain a stock solution of 0.3 mg/ml. Vehicle control consisted of 6 mM NaOH in saline. Twenty-week-old ADLP mice were injected intraperitoneally with 100 μl of vehicle or T_3 (corresponding to 1.0 mg/kg) 5 days per week for 8 weeks. For the injection of AMPCP (Tocris, no. 3633), 20-week-old *Cx3cr1*$^{gfp/+}$ mice received an intraperitoneal injection of 100 μl of vehicle (distilled water) or AMPCP (10 mg/kg) 5 days per week for 4 weeks. Eight-week-old ADLP$^{APP/PS1}$ mice received an intraperitoneal injection of 100 μl of vehicle (distilled water) or AMPCP (10 mg/kg) 5 days per week for 8 weeks to examine the change in amyloid pathology.

Live imaging using in vivo two-photon laser scanning microscopy

All animal studies and maintenance were approved by the Institutional Animal Care and Use Committee of Seoul National University, Korea. A thinned-skull window for live imaging was prepared by first anesthetizing mice by intramuscular injection of a tiletamine-zolazepam (Virbac) and xylazine (Bayer) mixture (1.2 mg/kg). The scalp and periosteum were removed, and then the skull was carefully thinned to a thickness of 15 to 20 μm using a microdrill. An LSM 7 MP system (Carl Zeiss) with a water-immersion objective lens (W Plan-Apochromat 20×/1.0 Differential Interference Contrast (DIC) M27 70 mm; Carl Zeiss) and Chameleon Ultra Titanium-Sapphire femtosecond laser (Coherent) was used for live imaging with two-photon laser scanning microscopy. Microglial green fluorescent protein signals were collected through a 500- to 555-nm Non-Descanned Detector (NDD) filter after excitation with a 920-nm laser. Following ablation of a focal (15 μm in diameter) brain region of interest by laser irradiation at a wavelength of 920 nm with 100% laser power, z-stack images (total depth, 50 μm; interval, 1 μm) were obtained every 1 min for 30 cycles. Microglial responses after laser ablation were analyzed as previously described (*25*). Briefly, all z-stack images were projected onto a single plane, and then two irradiated point–centered region of interest circles (outer circle, 140 μm in diameter; inner circle, 70 μm in diameter) were made on the plane. Response index at each time point was calculated as (inner circle fluorescence intensity$_t$ − inner circle fluorescence intensity$_0$)/outer circle fluorescence intensity$_0$. Two-photon laser scanning microscopy images were processed and analyzed using Volocity software (PerkinElmer).

Primary microglia culture

Primary microglial cells were prepared from newborn mouse pups (postnatal day 1; C57BL/6 mice). Cortices and hippocampi were scooped out from mouse pup brains and collected in ice-cold Hanks' balanced salt solution. After the meninges were carefully removed, the tissues were transferred to a 15-ml tube containing 3 ml of culture medium (DMEM containing fetal bovine serum and penicillin/streptomycin). The contents were triturated using a fire-polished Pasteur pipette and filtered through a 40-μm cell strainer. The resulting cells in culture medium were plated on Poly-D-Lysine (PDL)-coated T75 flasks, maintained in a 37°C, and humidified 5% CO_2 incubator for 11 to 12 days. At 11 to 12 days in vitro, floating microglial cells in T75 flasks were harvested and then replated at the appropriate density on PDL-coated plates for experiments.

Phagocytosis assay

Primary microglial cells (1.5×10^5 cells per well) were seeded into each well of a 12-well tissue culture plate, incubated at 37°C, and humidified 5% CO_2 incubator to stabilize and attach to the plate. To determine the phagocytic activity of microglia, pHrodo iFL Red (Thermo Fisher Scientific, P36014) was labeled for oligomer $A\beta_{1-42}$ according to the protocol provided by the manufacturer. After stabilizing microglia, T_3 was pretreated for 24 hours, followed by the treatment of 4 μM pHrodo iFL Red–labeled oligomer $A\beta_{1-42}$ with vehicle or 10 μM AMPCP for 24 hours. Since pHrodo iFL Red–labeled oligomer $A\beta_{1-42}$ turned red fluorescence (excitation/emission = 544/570) in the acidic microenvironment inside the cell, integrated red fluorescence intensity was recorded every hour for 24 hours by Image ExFluorer (Live Cell Instrument).

Bulk RNA-seq

Total RNA was collected from fresh mouse primary microglial cells from mice in vehicle and hypothyroidism groups and used to build next-generation RNA-seq libraries. The libraries were prepared using the TruSeq Stranded mRNA LT Sample Prep Kit. The generated libraries were sequenced on the Illumina Novaseq platform using paired-end 101–base pair reads reaching more than 50 million.

The resulting RNA-seq data were aligned to the mm10 mouse reference genome and normalized to fragments per kilobase of transcript per million mapped reads (FPKM) using RSEM-1.3.3. DEGs were identified using the edgeR-3.36.0 R package. After filtering for hypothyroidism-specific up-regulated and down-regulated genes with $P < 0.05$ and $\log_2$ fold change > 1, we identified 253 up-regulated and 133 down-regulated genes. The heatmap with FPKM z scores was sorted according to the GSEA S2N score for DEGs $|S2N| > 1.3$.

Single-cell RNA sequencing

Freshly isolated mouse hippocampi were dissociated into single cells using the Miltenyi Adult Brain Dissociation Kit on a gentleMACS Octo Dissociator with Heaters (37C ABDK 02 program). Dissociated cells were stained with the Fixable Viability Dye eFluor 660 (eBioscience), and viable cells free of debris were isolated using a BD FACSAria cell sorter (BD Biosciences). Before creating GEMs (gel-bead-in-emulsions), a 10x 3′ CellPlex Kit was used to multiplex all cells from four samples (CMO301, CMO302, CMO303, and CMO304). scRNA-seq libraries were constructed using the 10x Chromium Next GEM Single Cell 3′ Kit v3.1 and sequenced using the Illumina NovaSeq platform.

CellRanger 6.0.1 was used to align scRNA-seq data to the mouse reference genome mm10, and CellBender remove-background was used to remove background ambient RNA. After creating an object with Seurat 4.0.3 (*57*), cells with fewer than 500 genes or those with a mitochondrial gene content greater than 5% were excluded. SCTransform was used to normalize gene expression data, and all cells from the four sample groups were integrated using the canonical correlation analysis method. Cell types were determined by database-driven annotation using cell type–specific expression marker genes and the single-cell Mouse Cell Atlas (scMCA 0.2.0) (*58*). Monocle3 1.0.0 (*59*) calculates pseudotime for trajectory analysis of microglial cells.

Statistics

Data are presented as means ± SEM. Data with $P < 0.05$ were considered statistically significant. Two-tailed Student's t test, one-way analysis of variance (ANOVA), and two-way ANOVA with Tukey's post hoc test were performed in GraphPad Prism version 8.0.

Study approval

All animal experiments were conducted in accordance with the guidelines of and approved by the Institutional Animal Care and Use Committee of Seoul National University (SNU-190729-1).

Supplementary Materials

This PDF file includes:

Supplementary Text
Tables S1 and S2
Figs. S1 to S11
Legends for movies S1 to S4
References

Other Supplementary Material for this manuscript includes the following:

Movies S1 to S4

REFERENCES AND NOTES

1. 2022 Alzheimer's disease facts and figures. *Alzheimers Dement.* **18**, 700–789 (2022).
2. C. L. Masters, R. Bateman, K. Blennow, C. C. Rowe, R. A. Sperling, J. L. Cummings, Alzheimer's disease. *Nat. Rev. Dis. Primers* **1**, 15056 (2015).
3. M. S. Albert, Changes in cognition. *Neurobiol. Aging* **32** (Suppl. 1), S58–S63 (2011).
4. M. A. DeTure, D. W. Dickson, The neuropathological diagnosis of Alzheimer's disease. *Mol. Neurodegener.* **14**, 32 (2019).
5. M. P. Murphy, H. LeVine III, Alzheimer's disease and the β-amyloid peptide. *J. Alzheimers Dis.* **19**, 311–323 (2010).
6. J. C. Lambert, C. A. Ibrahim-Verbaas, D. Harold, A. C. Naj, R. Sims, C. Bellenguez, A. L. DeStafano, J. C. Bis, G. W. Beecham, B. Grenier-Boley, G. Russo, T. A. Thorton-Wells, N. Jones, A. V. Smith, V. Chouraki, C. Thomas, M. A. Ikram, D. Zelenika, B. N. Vardarajan, Y. Kamatani, C. F. Lin, A. Gerrish, H. Schmidt, B. Kunkle, M. L. Dunstan, A. Ruiz, M. T. Bihoreau, S. H. Choi, C. Reitz, F. Pasquier, C. Cruchaga, D. Craig, N. Amin, C. Berr, O. L. Lopez, P. L. De Jager, V. Deramecourt, J. A. Johnston, D. Evans, S. Lovestone, L. Letenneur, F. J. Moron, D. C. Rubinsztein, G. Eiriksdottir, K. Sleegers, A. M. Goate, N. Fievet, M. W. Huentelman, M. Gill, K. Brown, M. I. Kamboh, L. Keller, P. Barberger-Gateau, B. McGuiness, E. B. Larson, R. Green, A. J. Myers, C. Dufouil, S. Todd, D. Wallon, S. Love, E. Rogaeva, J. Gallacher, P. S. George-Hyslop, J. Clarimon, A. Lleo, A. Bayer, D. W. Tsuang, L. Yu, M. Tsolaki, P. Bossu, G. Spalletta, P. Proitsi, J. Collinge, S. Sorbi, F. Sanchez-Garcia, N. C. Fox, J. Hardy, M. C. D. Naranjo, P. Bosco, R. Clarke, C. Brayne, D. Galimberti, M. Mancuso, F. Matthews; European Alzheimer's Disease Initiative; Genetic and Environmental Risk in Alzheimer's Disease; Alzheimer's Disease Genetic Consortium, Cohorts for Heart and Aging Research in Genomic Epidemiology, S. Moebus, P. Mecocci, M. Del Zompo, W. Maier, H. Hampel, A. Pilotto, M. Bullido, F. Panza, P. Caffarra, B. Nacmias, J. R. Gilbert, M. Mayhaus, L. Lannefelt, H. Hakonarson, S. Pichler, M. M. Carrasquillo, M. Ingelsson, D. Beekly, V. Alvarez, F. Zou, O. Valladares, S. G. Younkin, E. Coto, K. L. Hamilton-Nelson, W. Gu, C. Razquin, P. Pastor, I. Mateo, M. J. Owen, K. M. Faber, P. V. Jonsson, O. Combarros, M. C. O'Donovan, L. B. Cantwell, H. Soininen, D. Blacker, S. Mead, T. H. Mosley Jr., D. A. Bennett, T. B. Harris, L. Fratiglioni, C. Holmes, R. F. de Bruijn, P. Passmore, T. J. Montine, K. Bettens, J. I. Rotter, A. Brice, K. Morgan, T. M. Foroud, W. A. Kukull, D. Hannequin, J. F. Powell, M. A. Nalls, K. Ritchie, K. L. Lunetta, J. S. Kauwe, E. Boerwinkle, M. Riemenschneider, M. Boada, M. Hiltuenen, E. R. Martin, R. Schmidt, D. Rujescu, L. S. Wang, J. F. Dartigues, R. Mayeux, C. Tzourio, A. Hofman, M. M. Nothen, C. Graff, B. M. Psaty, L. Jones, J. L. Haines, P. A. Holmans, M. Lathrop, M. A. Pericak-Vance, L. J. Launer, L. A. Farrer, C. M. van Duijn, C. Van Broeckhoven, V. Moskvina, S. Seshadri, J. Williams, G. D. Schellenberg, P. Amouyel, Meta-analysis of 74,046 individuals identifies 11 new susceptibility loci for Alzheimer's disease. *Nat. Genet.* **45**, 1452–1458 (2013).
7. G. D. Rabinovici, Late-onset Alzheimer disease. *Continuum (Minneap Minn)* **25**, 14–33 (2019).
8. D. K. Kim, I. Mook-Jung, The role of cell type-specific mitochondrial dysfunction in the pathogenesis of Alzheimer's disease. *BMB Rep.* **52**, 679–688 (2019).
9. M. J. Berridge, Calcium hypothesis of Alzheimer's disease. *Pflugers Arch.* **459**, 441–449 (2010).
10. H. Choi, H. J. Kim, J. Kim, S. Kim, J. Yang, W. Lee, Y. Park, S. J. Hyeon, D. S. Lee, H. Ryu, J. Chung, I. Mook-Jung, Increased acetylation of Peroxiredoxin1 by HDAC6 inhibition leads to recovery of Aβ-induced impaired axonal transport. *Mol. Neurodegener.* **12**, 23 (2017).

11. M. T. Heneka, M. J. Carson, J. El Khoury, G. E. Landreth, F. Brosseron, D. L. Feinstein, A. H. Jacobs, T. Wyss-Coray, J. Vitorica, R. M. Ransohoff, K. Herrup, S. A. Frautschy, B. Finsen, G. C. Brown, A. Verkhratsky, K. Yamanaka, J. Koistinaho, E. Latz, A. Halle, G. C. Petzold, T. Town, D. Morgan, M. L. Shinohara, V. H. Perry, C. Holmes, N. G. Bazan, D. J. Brooks, S. Hunot, B. Joseph, N. Deigendesch, O. Garaschuk, E. Boddeke, C. A. Dinarello, J. C. Breitner, G. M. Cole, D. T. Golenbock, M. P. Kummer, Neuroinflammation in Alzheimer's disease. *Lancet Neurol.* **14**, 388–405 (2015).
12. Y. Peng, P. Gao, L. Shi, L. Chen, J. Liu, J. Long, Central and peripheral metabolic defects contribute to the pathogenesis of Alzheimer's disease: Targeting mitochondria for diagnosis and prevention. *Antioxid. Redox Signal.* **32**, 1188–1236 (2020).
13. J. Bernal, "THYROID HORMONES IN THE DEVELOPING BRAIN" in Thyroid hormones in brain development and function, in *Endotext*, K. R. Feingold, B. Anawalt, A. Boyce, G. Chrousos, W. W. de Herder, K. Dhatariya, K. Dungan, J. M. Hershman, J. Hofland, S. Kalra, G. Kaltsas, C. Koch, P. Kopp, M. Korbonits, C. S. Kovacs, W. Kuohung, B. Laferrere, M. Levy, E. A. McGee, R. McLachlan, J. E. Morley, M. New, J. Purnell, R. Sahay, F. Singer, M. A. Sperling, C. A. Stratakis, D. L. Trence, D. P. Wilson, Eds. (MDText.com Inc., 2000).
14. R. Mullur, Y. Y. Liu, G. A. Brent, Thyroid hormone regulation of metabolism. *Physiol. Rev.* **94**, 355–382 (2014).
15. J. Bernal, Thyroid hormone receptors in brain development and function. *Nat. Clin. Pract. Endocrinol. Metab.* **3**, 249–259 (2007).
16. M. D. Hartley, T. Banerji, I. J. Tagge, L. L. Kirkemo, P. Chaudhary, E. Calkins, D. Galipeau, M. D. Shokat, M. J. DeBell, S. Van Leuven, H. Miller, G. Marracci, E. Pocius, T. Banerji, S. J. Ferrara, J. M. Meinig, B. Emery, D. Bourdette, T. S. Scanlan, Myelin repair stimulated by CNS-selective thyroid hormone action. *JCI Insight* **4**, e126329 (2019).
17. B. Malekpour, A. Mehrafshan, F. Saki, Z. Malekmohammadi, N. Saki, Effect of posttraumatic serum thyroid hormone levels on severity and mortality of patients with severe traumatic brain injury. *Acta Med. Iran.* **50**, 113–116 (2012).
18. C. Lin, N. Li, H. Chang, Y. Shen, Z. Li, W. Wei, H. Chen, H. Lu, J. Ji, N. Liu, Dual effects of thyroid hormone on neurons and neurogenesis in traumatic brain injury. *Cell Death Dis.* **11**, 671 (2020).
19. A. E. Kincaid, Spontaneous circling behavior and dopamine neuron loss in a genetically hypothyroid mouse. *Neuroscience* **105**, 891–898 (2001).
20. C. Rieben, D. Segna, B. R. da Costa, T. H. Collet, L. Chaker, C. E. Aubert, C. Baumgartner, O. P. Almeida, E. Hogervorst, S. Trompet, K. Masaki, S. P. Mooijaart, J. Gussekloo, R. P. Peeters, D. C. Bauer, D. Aujesky, N. Rodondi, Subclinical thyroid dysfunction and the risk of cognitive decline: A meta-analysis of prospective cohort studies. *J. Clin. Endocrinol. Metab.* **101**, 4945–4954 (2016).
21. M. Eslami-Amirabadi, S. A. Sajjadi, The relation between thyroid dysregulation and impaired cognition/behaviour: An integrative review. *J. Neuroendocrinol.* **33**, e12948 (2021).
22. B. W. Choi, S. Kim, S. Kang, K. S. Won, H. A. Yi, H. W. Kim, Relationship between thyroid hormone levels and the pathology of Alzheimer's disease in euthyroid subjects. *Thyroid* **30**, 1547–1555 (2020).
23. H. J. Choi, M. S. Byun, D. Yi, B. K. Sohn, J. H. Lee, J. Y. Lee, Y. K. Kim, D. Y. Lee, K. R. Group, Associations of thyroid hormone serum levels with in-vivo Alzheimer's disease pathologies. *Alzheimers Res. Ther.* **9**, 64 (2017).
24. J. D. Davis, A. Podolanczuk, J. E. Donahue, E. Stopa, J. V. Hennessey, L. G. Luo, Y. P. Lim, R. A. Stern, Thyroid hormone levels in the prefrontal cortex of post-mortem brains of Alzheimer's disease patients. *Curr. Aging Sci.* **1**, 175–181 (2008).
25. S. H. Baik, S. Kang, W. Lee, H. Choi, S. Chung, J. I. Kim, I. Mook-Jung, A breakdown in metabolic reprogramming causes microglia dysfunction in Alzheimer's disease. *Cell Metab.* **30**, 493–507.e6 (2019).
26. R. J. Denver, K. E. Williamson, Identification of a thyroid hormone response element in the mouse Kruppel-like factor 9 gene to explain its postnatal expression in the brain. *Endocrinology* **150**, 3935–3943 (2009).
27. A. Engelhard, A. M. Christiano, The hairless promoter is differentially regulated by thyroid hormone in keratinocytes and neuroblastoma cells. *Exp. Dermatol.* **13**, 257–264 (2004).
28. B. Gereben, A. Zeold, M. Dentice, D. Salvatore, A. C. Bianco, Activation and inactivation of thyroid hormone by deiodinases: Local action with general consequences. *Cell. Mol. Life Sci.* **65**, 570–590 (2008).
29. C. Luongo, M. Dentice, D. Salvatore, Deiodinases and their intricate role in thyroid hormone homeostasis. *Nat. Rev. Endocrinol.* **15**, 479–488 (2019).
30. M. Dentice, D. Salvatore, Deiodinases: The balance of thyroid hormone: Local impact of thyroid hormone inactivation. *J. Endocrinol.* **209**, 273–282 (2011).
31. W. E. Visser, E. C. Friesema, T. J. Visser, Minireview: Thyroid hormone transporters: The knowns and the unknowns. *Mol. Endocrinol.* **25**, 1–14 (2011).
32. F. R. Lima, A. Gervais, C. Colin, M. Izembart, V. M. Neto, M. Mallat, Regulation of microglial development: A novel role for thyroid hormone. *J. Neurosci.* **21**, 2028–2038 (2001).
33. Y. Mori, D. Tomonaga, A. Kalashnikova, F. Furuya, N. Akimoto, M. Ifuku, Y. Okuno, K. Beppu, K. Fujita, T. Katafuchi, H. Shimura, L. P. Churilov, M. Noda, Effects of 3,3′,5-triiodothyronine on microglial functions. *Glia* **63**, 906–920 (2015).
34. M. J. Chen, S. Ramesha, L. D. Weinstock, T. Gao, L. Ping, H. Xiao, E. B. Dammer, D. D. Duong, A. I. Levey, J. J. Lah, N. T. Seyfried, L. B. Wood, S. Rangaraju, Extracellular signal-regulated kinase regulates microglial immune responses in Alzheimer's disease. *J. Neurosci. Res.* **99**, 1704–1721 (2021).
35. C. C. Chao, S. Hu, T. W. Molitor, E. G. Shaskan, P. K. Peterson, Activated microglia mediate neuronal cell injury via a nitric oxide mechanism. *J. Immunol.* **149**, 2736–2741 (1992).
36. J. E. Yuste, E. Tarragon, C. M. Campuzano, F. Ros-Bernal, Implications of glial nitric oxide in neurodegenerative diseases. *Front. Cell. Neurosci.* **9**, 322 (2015).
37. C. Y. Lee, G. E. Landreth, The role of microglia in amyloid clearance from the AD brain. *J. Neural Transm. (Vienna)* **117**, 949–960 (2010).
38. S. H. Baik, S. Kang, S. M. Son, I. Mook-Jung, Microglia contributes to plaque growth by cell death due to uptake of amyloid β in the brain of Alzheimer's disease mouse model. *Glia* **64**, 2274–2290 (2016).
39. H. Keren-Shaul, A. Spinrad, A. Weiner, O. Matcovitch-Natan, R. Dvir-Szternfeld, T. K. Ulland, E. David, K. Baruch, D. Lara-Astaiso, B. Toth, S. Itzkovitz, M. Colonna, M. Schwartz, I. Amit, A unique microglia type associated with restricting development of Alzheimer's disease. *Cell* **169**, 1276–1290.e17 (2017).
40. A. Deczkowska, H. Keren-Shaul, A. Weiner, M. Colonna, M. Schwartz, I. Amit, Disease-associated microglia: A universal immune sensor of neurodegeneration. *Cell* **173**, 1073–1081 (2018).
41. D. G. Walker, L. F. Lue, Immune phenotypes of microglia in human neurodegenerative disease: Challenges to detecting microglial polarization in human brains. *Alzheimers Res. Ther.* **7**, 56 (2015).
42. A. Young, S. F. Ngiow, D. S. Barkauskas, E. Sult, C. Hay, S. J. Blake, Q. Huang, J. Liu, K. Takeda, M. W. L. Teng, K. Sachsenmeier, M. J. Smyth, Co-inhibition of CD73 and A2AR adenosine signaling improves anti-tumor immune responses. *Cancer Cell* **30**, 391–403 (2016).
43. S. P. Colgan, H. K. Eltzschig, T. Eckle, L. F. Thompson, Physiological roles for ecto-5′-nucleotidase (CD73). *Purinergic Signal* **2**, 351–360 (2006).
44. S. Y. Neo, Y. Yang, J. Record, R. Ma, X. Chen, Z. Chen, N. P. Tobin, E. Blake, C. Seitz, R. Thomas, A. K. Wagner, J. Andersson, J. de Boniface, J. Bergh, S. Murray, E. Alici, R. Childs, M. Johansson, L. S. Westerberg, F. Haglund, J. Hartman, A. Lundqvist, CD73 immune checkpoint defines regulatory NK cells within the tumor microenvironment. *J. Clin. Invest.* **130**, 1185–1198 (2020).
45. M. Yu, G. Guo, L. Huang, L. Deng, C. S. Chang, B. R. Achyut, M. Canning, N. Xu, A. S. Arbab, R. J. Bollag, P. C. Rodriguez, A. L. Mellor, H. Shi, D. H. Munn, Y. Cui, CD73 on cancer-associated fibroblasts enhanced by the A2B-mediated feedforward circuit enforces an immune checkpoint. *Nat. Commun.* **11**, 515 (2020).
46. M. R. Wink, A. S. Tamajusuku, E. Braganhol, E. A. Casali, M. L. Barreto-Chaves, J. J. Sarkis, A. M. Battastini, Thyroid hormone upregulates ecto-5′-nucleotidase/CD73 in C6 rat glioma cells. *Mol. Cell. Endocrinol.* **205**, 107–114 (2003).
47. A. S. Tamajusuku, M. A. Carrillo-Sepulveda, E. Braganhol, M. R. Wink, J. J. Sarkis, M. L. Barreto-Chaves, A. M. Battastini, Activity and expression of ecto-5′-nucleotidase/CD73 are increased by thyroid hormones in vascular smooth muscle cells. *Mol. Cell. Biochem.* **289**, 65–72 (2006).
48. M. S. Carneiro-Ramos, V. B. da Silva, M. B. Coutinho Jr., A. M. Battastini, J. J. Sarkis, M. L. Barreto-Chaves, Thyroid hormone stimulates 5′-ecto-nucleotidase of neonatal rat ventricular myocytes. *Mol. Cell. Biochem.* **265**, 195–201 (2004).
49. L. Chaker, A. C. Bianco, J. Jonklaas, R. P. Peeters, Hypothyroidism. *Lancet* **390**, 1550–1562 (2017).
50. E. A. McAninch, S. Jo, N. Z. Preite, E. Farkas, P. Mohacsik, C. Fekete, P. Egri, B. Gereben, Y. Li, Y. Deng, M. E. Patti, C. Zevenbergen, R. P. Peeters, D. C. Mash, A. C. Bianco, Prevalent polymorphism in thyroid hormone-activating enzyme leaves a genetic fingerprint that underlies associated clinical syndromes. *J. Clin. Endocrinol. Metab.* **100**, 920–933 (2015).
51. S. Jo, T. L. Fonseca, B. Bocco, G. W. Fernandes, E. A. McAninch, A. P. Bolin, R. R. Da Conceicao, J. P. Werneck-de-Castro, D. L. Ignacio, P. Egri, D. Nemeth, C. Fekete, M. M. Bernardi, V. D. Leitch, N. S. Mannan, K. F. Curry, N. C. Butterfield, J. H. D. Bassett, G. R. Williams, B. Gereben, M. O. Ribeiro, A. C. Bianco, Type 2 deiodinase polymorphism causes ER stress and hypothyroidism in the brain. *J. Clin. Invest.* **129**, 230–245 (2019).
52. M. Mallat, F. R. Lima, A. Gervais, C. Colin, V. Moura Neto, New insights into the role of thyroid hormone in the CNS: The microglial track. *Mol. Psychiatry* **7**, 7–8 (2002).
53. M. Noda, Possible role of glial cells in the relationship between thyroid dysfunction and mental disorders. *Front. Cell. Neurosci.* **9**, 194 (2015).
54. D. Allard, B. Allard, P. Gaudreau, P. J. Stagg, CD73–adenosine: A next-generation target in immuno-oncology. *Immunotherapy* **8**, 145–163 (2016).
55. A. Badimon, H. J. Strasburger, P. Ayata, X. Chen, A. Nair, A. Ikegami, P. Hwang, A. T. Chan, S. M. Graves, J. O. Uweru, C. Ledderose, M. G. Kutlu, M. A. Wheeler, A. Kahan, M. Ishikawa, Y. C. Wang, Y. E. Loh, J. X. Jiang, D. J. Surmeier, S. C. Robson, W. G. Junger, R. Sebra, E. S. Calipari, P. J. Kenny, U. B. Eyo, M. Colonna, F. J. Quintana, H. Wake, V. Gradinaru, A. Schaefer, Negative feedback control of neuronal activity by microglia. *Nature* **586**, 417–423 (2020).

56. D. K. Kim, J. Park, D. Han, J. Yang, A. Kim, J. Woo, Y. Kim, I. Mook-Jung, Molecular and functional signatures in a novel Alzheimer's disease mouse model assessed by quantitative proteomics. *Mol. Neurodegener.* **13**, 2 (2018).
57. Y. Hao, S. Hao, E. Andersen-Nissen, W. M. Mauck III, S. Zheng, A. Butler, M. J. Lee, A. J. Wilk, C. Darby, M. Zager, P. Hoffman, M. Stoeckius, E. Papalexi, E. P. Mimitou, J. Jain, A. Srivastava, T. Stuart, L. M. Fleming, B. Yeung, A. J. Rogers, J. M. McElrath, C. A. Blish, R. Gottardo, P. Smibert, R. Satija, Integrated analysis of multimodal single-cell data. *Cell* **184**, 3573–3587.e29 (2021).
58. X. Han, R. Wang, Y. Zhou, L. Fei, H. Sun, S. Lai, A. Saadatpour, Z. Zhou, H. Chen, F. Ye, D. Huang, Y. Xu, W. Huang, M. Jiang, X. Jiang, J. Mao, Y. Chen, C. Lu, J. Xie, Q. Fang, Y. Wang, R. Yue, T. Li, H. Huang, S. H. Orkin, G. C. Yuan, M. Chen, G. Guo, Mapping the mouse cell atlas by microwell-seq. *Cell* **172**, 1091–1107.e17 (2018).
59. J. Cao, M. Spielmann, X. Qiu, X. Huang, D. M. Ibrahim, A. J. Hill, F. Zhang, S. Mundlos, L. Christiansen, F. J. Steemers, C. Trapnell, J. Shendure, The single-cell transcriptional landscape of mammalian organogenesis. *Nature* **566**, 496–502 (2019).
60. J. C. Park, S. Y. Jang, D. Lee, J. Lee, U. Kang, H. Chang, H. J. Kim, S. H. Han, J. Seo, M. Choi, D. Y. Lee, M. S. Byun, D. Yi, K. H. Cho, I. Mook-Jung, A logical network-based drug-screening platform for Alzheimer's disease representing pathological features of human brain organoids. *Nat. Commun.* **12**, 280 (2021).

Acknowledgments

Funding: This research was supported by a grant from the Korea Health Technology R&D Project through the Korea Health Industry Development Institute (KHIDI) and Korea Dementia Research Center (KDRC), funded by the Ministry of Health and Welfare and Ministry of Science and ICT, Republic of Korea (grant numbers HU20C0187 to I.M.-J. and HU23C1234 to H.R.). The work was also supported by grants from the National Research Foundation of Korea (NRF-2020R1A6A3A13068606 and NRF-2021R1A6A3A01087248) to Hyunjung Choi. Analysis of sequencing data was mostly carried out using the computing server at the Genomic Medicine Institute Research Service Center. **Author contributions:** D.K.K., Hyunjung Choi, and I.M.-J. designed and conceptualized the study. W.L. and J.-I.K. performed and analyzed scRNA-seq and bulk RNA-seq data. Hayoung Choi imaged microglial motility in vivo by two-photon microscopy. D.K.K., Hyunjung Choi, S.B.H., and J.H. performed animal experiments. D.K.K., Hyunjung Choi, and J.-H.J. performed and analyzed in vitro microglial culture experiments. D.K.K., Hyunjung Choi, and H.R. analyzed immunostaining of human AD patient brains. Hyunjung Choi and J.W.H. performed and analyzed human AD brain organoid experiments. D.K.K., Hyunjung Choi, and I.M.-J. wrote and reviewed the manuscript. All authors read and approved the final manuscript. **Competing interests:** The authors declared that they have no competing interests. **Data and materials availability:** scRNA-seq and microglia bulk RNA-seq data were deposited in NCBI's Gene Expression Omnibus under accession number GSE219131. All data needed to evaluate the conclusions in the paper are present in the paper and/or the Supplementary Materials.

Submitted 10 April 2023
Accepted 12 February 2024
Published 15 March 2024
10.1126/sciadv.adi1863